Available online at www.sciencedirect.com
SCIENCE DIRECT®
ELSEVIER
European Journal of Mechanics B/Fluids 23 (2004) 501–518
EUROPEAN JOURNAL OF MECHANICS B/FLUIDS

Turbulent flow over a swept backward-facing step

Hans-Jakob Kaltenbach

Hermann-Föttinger-Institut, Technische Universität Berlin, Sekretariat HF 1, Strasse des 17. Juni 135, 10623 Berlin, Germany

Received 1 February 2003; accepted 30 October 2003

Abstract

The spanwise invariant flow over a swept, backward-facing step of height H at $Re_H = C_0 H/\nu = 5000$ with turbulent upstream conditions has been studied for sweep angles up to $\alpha = 70^\circ$ using large-eddy simulation. The reattachment length $x_R \approx 6.2$ H remains nearly constant up to $\alpha = 30^\circ$, decreases for larger sweep angles, and reaches $x_R \approx 4.0$ H for $\alpha = 70^\circ$. Step-normal components $U/(C_0 \cos\alpha)$ and edge-parallel components $W/(C_0 \sin\alpha)$ of the mean flow show approximate collapse for $\alpha \leqslant 50^\circ$ if compared at the same location x/x_R. However, the sweep-independence principle does not hold in a strict sense since the scaling of the momentum budgets undergoes significant changes with streamwise distance from the step. Dynamics in the first half of the separation region are strongly influenced by the scaling relations imposed by the upstream conditions. In accordance with the momentum integral theorem the overall pressure rise scales as $(C_0 \cos\alpha)^2$ which partially explains why several quantities tend to scale near reattachment as if the flow were sweep independent. No significant influence of the mean flow skewing on the statistical turbulence structure is observed inside the free shear layer emanating from the edge. Conversely, introduction of sweep causes substantial changes in the dynamics of the near-wall region upstream of reattachment.

Keywords: Turbulence; Separation; Three-dimensional; Skewing; Backward-facing step

1. Introduction

1.1. Motivation and background

Most flows of engineering interest have regions where the mean flow is three-dimensional (3D), i.e., carries axial vorticity. Consider an initially two-dimensional turbulent boundary layer (2D-TBL) which due to a spanwise shear imposed at the wall or due to a pressure gradient is forced to turn sidewise. The resulting profile of the mean velocity is three-dimensional or 'skewed'. With respect to the local coordinates $\hat{x},\ \hat{y},\ \hat{z}$ aligned with a potential flow streamline at the edge of the boundary layer the flow develops a 'cross-flow' component $\widehat{W}$. For such a situation, turbulence modeling is complicated by the presence of additional strain rates together with the often observed misalignment of the shear-stress vector $(\rho\langle\hat{u}'\hat{v}'\rangle, \rho\langle\hat{v}'\hat{w}'\rangle)$ and velocity-gradient vector $(\partial\widehat{U}/\partial y, \partial\widehat{W}/\partial y)$.

The 3D-TBL has been the subject of a number of studies with the objective to identify effects of mean flow three-dimensionality on the turbulence structure, see Johnston and Flack [1] and Coleman et al. [2] for recent reviews. Several of these studies were clouded by the fact that axial vorticity often arises simultaneously with streamwise changes in pressure and/or streamline curvature which are also known to affect turbulence. The identification of pure effects from mean-flow skewing requires sophisticated arrangements, such as in the numerical simulation study by Coleman et al. [2]. They showed that the statistical turbulence structure in the outer layer of a TBL hardly changes if it is subject to a pure skewing-type, irrotational strain rate in the wall-parallel plane. Similar conclusions were drawn from the analysis of the 3D flow over a swept bump by Webster et al. [3] and Wu and Squires [4].

E-mail address: kaltenbach@pi.tu-berlin.de (H.-J. Kaltenbach).

0997-7546/$ – see front matter
doi:10.1016/j.euromechflu.2003.10.015

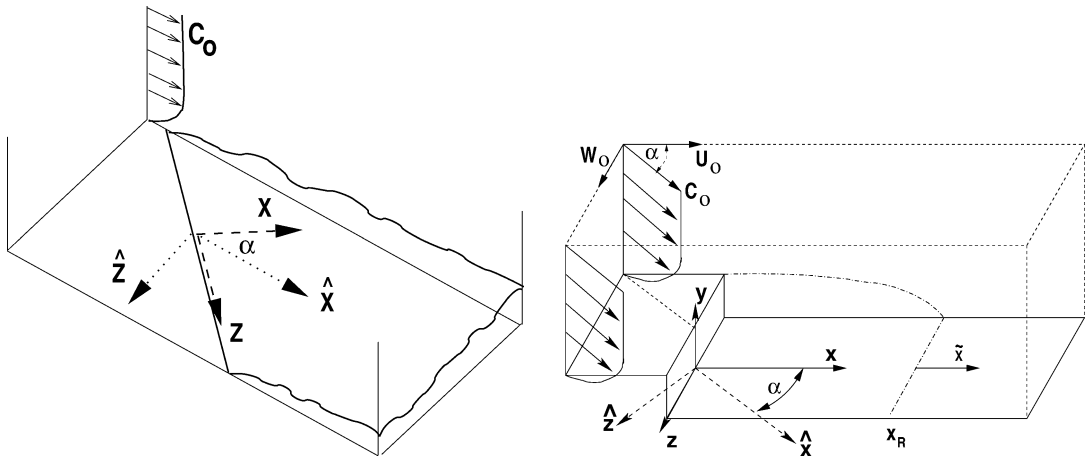

Fig. 1. Left: Co-planar turbulent boundary layer evolving downstream of a swept transition device. The flow is homogeneous along the coordinate z. Right: Sketch of the computational domain. The free stream of magnitude C_0 forms the angle α with respect to the step-normal direction. Both, step-aligned coordinates $x,\ y,\ z$ and free-stream aligned coordinates $\hat{x},\ \hat{y},\ \hat{z}$ (where $\hat{y} = y$ holds) will be used.

Testing of model assumptions requires knowledge of detailed turbulence statistics. For 3D flows with separation, few extensive measurements for all components of the Reynolds stress tensor are currently available. Databases from high-resolution numerical simulation (direct and large-eddy simulation, respectively DNS and LES) can partially bridge this gap. The flow over a backward-facing step of height H, where the free-stream direction is no longer perpendicular to the step edge as sketched in Fig. 1, is one of the simplest geometrical configurations which allows one to study a 3D flow with separation. The most general configuration results from the assumption of homogeneity or 'spanwise' invariance along the step edge. In the laboratory, spanwise invariance of the properties of the swept, co-planar TBL approaching the edge is achieved by either letting it grow along a plate with swept-back leading edge or by the use of a swept transition device as in the experiment of [3].

1.2. Sweep independence and scaling relations

The mean momentum balances for the incompressible turbulent flow in coordinates $x,\ y,\ z$ aligned with the step edge, using the Reynolds decomposition $u_i = U_i + u_i'$ where the mean is denoted as $\langle u_i \rangle \equiv U_i$, and assuming homogeneity along z, read

$$U\frac{\partial U}{\partial x} + V\frac{\partial U}{\partial y} = -\frac{\partial \langle u'^2 \rangle}{\partial x} - \frac{\partial \langle u'v' \rangle}{\partial y} - \frac{1}{\rho}\frac{\partial P}{\partial x} + \nu\left(\frac{\partial^2 U}{\partial x^2} + \frac{\partial^2 U}{\partial y^2}\right), \tag{1}$$

$$U\frac{\partial V}{\partial x} + V\frac{\partial V}{\partial y} = -\frac{\partial \langle u'v' \rangle}{\partial x} - \frac{\partial \langle v'^2 \rangle}{\partial y} - \frac{1}{\rho}\frac{\partial P}{\partial y} + \nu\left(\frac{\partial^2 V}{\partial x^2} + \frac{\partial^2 V}{\partial y^2}\right), \tag{2}$$

$$U\frac{\partial W}{\partial x} + V\frac{\partial W}{\partial y} = -\frac{\partial \langle u'w' \rangle}{\partial x} - \frac{\partial \langle v'w' \rangle}{\partial y} + \nu\left(\frac{\partial^2 W}{\partial x^2} + \frac{\partial^2 W}{\partial y^2}\right). \tag{3}$$

The sweep-independence principle states that Eqs. (1) and (2) are independent of the presence and strength of the step-parallel component W which satisfies a transport equation for a passive scalar. Strict sweep independence is possible only if the flow is laminar, i.e., the Reynolds stress terms in Eqs. (1)–(3) vanish. Deviations from the sweep-independence principle in a turbulent flow result from the coupling of the balance equations for the second moments through pressure-strain and dissipation rate terms.

Several consequences arise from strict sweep independence: (i) the location x_R of the reattachment line does not vary with sweep angle α; (ii) mean flow profiles at the same x collapse in the normalization $U/U_0,\ V/U_0$, and W/W_0 where $U_0 = C_0\cos\alpha$ and $W_0 = C_0\sin\alpha$ denote step-normal and step-parallel components of the free stream C_0; (iii) the pressure coefficient $c_p = (P - P_0)/P_{\mathrm{dyn}}$ does not change with α if the dynamic pressure P_{dyn} is formed with U_0^2; (iv) each term in Eqs. (1) and (2) scales on $C_0^2\cos^2\alpha L_0^{-1}$ and each term in Eq. (3) scales on $C_0^2\cos\alpha\sin\alpha L_0^{-1}$; here, L_0 is a characteristic length scale of the flow in the x, y-plane such as the step height H; (v) from (iv) follows that the 'step-normal' Reynolds number $Re_\alpha = HU_0/\nu = H(C_0\cos\alpha)/\nu$ must be held constant.

The scaling relations (iv) become evident if the sweep-independent solution for the velocity field

$$\mathbf{U}(x,y)=\begin{pmatrix}U(x,y)\\V(x,y)\\W(x,y)\end{pmatrix}=\begin{pmatrix}g_1(x,y)U_0\\g_2(x,y)U_0\\g_3(x,y)W_0\end{pmatrix}=\begin{pmatrix}g_1(x,y)C_0\cos\alpha\\g_2(x,y)C_0\cos\alpha\\g_3(x,y)C_0\sin\alpha\end{pmatrix}=E_{ij}g_j\,C_0 \tag{4}$$

is factored into the dimensionless functions $g_i(x,y)$, the reference velocity C_0, and the 'scale factors' E_{ij} where the only non-zero elements of E_{ij} read $E_{11}=\cos\alpha,\ E_{22}=\cos\alpha$, and $E_{33}=\sin\alpha$. Thus, the left-hand side of Eqs. (1)–(3) can be expressed as

$$\begin{aligned}\partial U_iU_j/\partial x_j=E_{im}E_{jn}f_{mn}(x,y)C_0^2&=\begin{pmatrix}\cos^2\alpha f_{11}&\cos^2\alpha f_{12}&\cos\alpha\sin\alpha f_{13}\\\cos^2\alpha f_{21}&\cos^2\alpha f_{22}&\cos\alpha\sin\alpha f_{23}\\\cos\alpha\sin\alpha f_{31}&\cos\alpha\sin\alpha f_{32}&\sin^2\alpha f_{33}\end{pmatrix}C_0^2\\&=\begin{pmatrix}[U_0^2]f_{11}&[U_0^2]f_{12}&[U_0W_0]f_{13}\\[U_0^2]f_{21}&[U_0^2]f_{22}&[U_0W_0]f_{23}\\[U_0W_0]f_{31}&[U_0W_0]f_{32}&[W_0^2]f_{33}\end{pmatrix},\end{aligned} \tag{5}$$

i.e., the product of a non-dimensional, sweep-independent part $f_{mn}(x,y)$, the square C_0^2 of the reference velocity, and the product $E_{im}E_{jn}$ of 'scale factors'. Formally, Eq. (5) indicates that the scaling conditions summarized in (iv) are violated by the entries of the third column of the matrix. This, however, does not preclude sweep independence since the corresponding terms do not contribute to Eqs. (1)–(3) because of the homogeneity along z.

Strict sweep independence requires that any second rank tensor which appears in divergence form $\partial T_{ij}/\partial x_j$ on the right hand of Eqs. (1)–(3) can be factored in a similar manner as Eq. (5). Thus, from the scaling behaviour of individual tensor components it can be judged to what degree the flow follows the sweep independence principle. For example, if the dominant Reynolds stress terms in Eqs. (1) and (3) satisfy condition (iv), i.e., $\partial\langle u'v'\rangle/\partial y$ scales on $U_0^2L_0^{-1}$ and $\partial\langle v'w'\rangle/\partial y$ scales on $U_0W_0L_0^{-1}$, the relations (ii) and (iii) can still be valid in a turbulent flow. This was found to be approximately the case for a swept flow in which the shear layer undergoes transition [5].

Now we turn our attention to the scaling properties of the configuration sketched in Fig. 1, in which a co-planar turbulent boundary layer evolves under a zero pressure gradient along a flat plate and approaches the swept-back edge of a step. There exists a fundamental difference between the laminar and the turbulent case with respect to the scaling properties of the incoming boundary layer: the basic requirement for strict sweep-independence, namely to keep the boundary layer thickness δ_{99}/H, the shape factor H_{12}, and the x-component $\tau_{w,x}=\rho\nu\partial U/\partial y$ of the wall shear stress at a constant value when the free-stream direction is no longer aligned with x, is imposed in the laminar case by increasing the free stream Reynolds number $Re_H=C_0H/\nu$ by the factor $1/\cos\alpha$.

For a TBL the Reynolds number dependence of c_f is much weaker than in the laminar case. This precludes the option to prescribe simultaneously $\delta_{99},\ H_{12}$, and $c_{f,x}=\tau_{w,x}/(\rho U_0^2)$ at the domain inlet in case of turbulent inflow. Therefore, we choose to conduct the present study at a constant value of $c_f=\tau_W/(0.5\rho C_0^2)$ by keeping the free-stream based Reynolds number Re_H at a fixed value for all sweep angles.

Even for these conditions it is not entirely clear to what degree the properties of a co-planar TBL are invariant with respect to the sweep angle. For laminar flow under zero pressure gradient Eq. (3) becomes formally identical to Eq. (1) if W is replaced by U, implying that $U(x,y)/U_0=W(x,y)/W_0$, i.e., an invariant mean-flow profile. It is not obvious whether the same holds in the turbulent case since the emergence of the (weak) rotational strain-rate $S_{13}=-\Omega_{13}=0.5\partial W/\partial x$ might influence the evolution of turbulence. As a consequence, subtle differences might exist among the mean flow profiles of the swept and the un-swept case even for the zero pressure-gradient TBL.

Nevertheless, in order to arrive at some estimates for the scaling relations that characterize the turbulent inflow for $Re_H=const.$, we assume that the mean velocity vector and the Reynolds stress tensor in a co-planar TBL take the form

$$\mathbf{U}(\hat{x},\hat{y})=\begin{pmatrix}\widehat{U}\\\widehat{V}\\0\end{pmatrix}=\begin{pmatrix}h_1\\h_2\\0\end{pmatrix}C_0\quad\text{and}\quad\langle\hat{u}_i'\hat{u}_j'\rangle=\begin{pmatrix}r_{11}&r_{12}&r_{13}\\r_{12}&r_{22}&0\\r_{13}&0&r_{33}\end{pmatrix}C_0^2 \tag{6}$$

with respect to the coordinates $\hat{x},\ \hat{y},\ \hat{z}$. The solution has been split into the reference scales C_0, respectively C_0^2, and the non-dimensional functions $h_i(\hat{x},\hat{y})$ and $r_{ij}(\hat{x},\hat{y})$ which are assumed to be approximately invariant with respect to α. The tensor component r_{13} has been included since from the momentum balance with respect to $\hat{z}$ follows under the assumptions $\partial P/\partial\hat{z}=0,\ \widehat{W}=0$, and $\langle\hat{v}'\hat{w}'\rangle=0$ that $-\partial\langle\hat{u}'\hat{w}'\rangle/\partial\hat{x}$ has to balance $\partial\langle\hat{w}'\hat{w}'\rangle/\partial\hat{z}$. Otherwise, a weak cross flow $\widehat{W}\neq0$ would be induced by the Reynolds stress gradients similarly to the secondary flow encountered in corners of ducts [6].

The components of the co-planar flow defined in Eq. (6) decomposed with respect to x, y, z read

$$\mathbf{U} = \begin{pmatrix} U \\ V \\ W \end{pmatrix} = \begin{pmatrix} h_1 C_0 \cos\alpha \\ h_2 C_0 \\ h_1 C_0 \sin\alpha \end{pmatrix} = \begin{pmatrix} h_1 U_0 \\ h_2 C_0 \\ h_1 W_0 \end{pmatrix}. \tag{7}$$

Note, that this scaling differs from Eq. (4) with respect to V. The components of the corresponding Reynolds stress tensor read

$$\begin{aligned}
\langle u'u' \rangle &= \left[\cos^2\alpha r_{11} - 2\sin\cos\alpha r_{13} + \sin^2\alpha r_{33}\right] C_0^2, \\
\langle v'v' \rangle &= r_{22}\left[C_0^2\right], \\
\langle w'w' \rangle &= \left[\sin^2\alpha r_{11} + 2\sin\cos\alpha r_{13} + \cos^2\alpha r_{33}\right] C_0^2, \\
\langle u'w' \rangle &= \left[-\sin\alpha\cos\alpha\,(r_{11} - r_{33}) + \left(\cos^2\alpha - \sin^2\alpha\right) r_{13}\right] C_0^2, \\
\langle u'v' \rangle &= r_{12} C_0^2 \cos\alpha = r_{12}[U_0 C_0], \\
\langle v'w' \rangle &= r_{12} C_0^2 \sin\alpha = r_{12}[W_0 C_0].
\end{aligned} \tag{8}$$

Unlike for Eq. (5) it is not possible to factor each tensor component of Eq. (8) into a product of velocity scales and a function which is invariant with respect to α. Nevertheless, the subset of the three tensor components $\langle v'v' \rangle$, $\langle u'v' \rangle$, and $\langle v'w' \rangle$ admits such a factorization. Since the corresponding 'scaling' differs from the one derived in Eq. (5) the comparison of normalized profiles of these stress tensor components helps to distinguish regions which scale like the incoming TBL from regions which scale according to the sweep-independence principle.

1.3. Previous work and goals of the present study

Some measurements are available for either a laminar or a turbulent boundary layer approaching a swept step [7–9]. Closely related are the investigations of swept separation bubbles forming behind fences or along blunt plates [10–12]. A common finding among these studies is the observation that the reattachment length x_R remains independent of sweep angle up to $\alpha \approx 40°$ and decreases for higher angles. For the swept bubble forming along a blunt plate Barkey Wolf [10] observed that both the static pressure and the r.m.s. of wall pressure fluctuations scale on the free stream velocity component $U_0 = C_0 \cos\alpha$ normal to the leading edge.

The present study extends previous work [5,13,14] which dealt with separation and transition of a laminar shear layer behind the edge of a swept, backward-facing step. We briefly summarize the main findings of this study in which α was varied between $0°$ and $60°$ keeping the 'step-normal' Reynolds number fixed at $Re_\alpha = 3000$: transition of the free shear layer behind the step is dominated by a Kelvin–Helmholtz type instability where the most amplified wave is roughly normal to the direction of the incoming flow. In accordance with the measurements of Fernholz et al. [7], the sweep independence principle holds up to $\alpha \approx 40°$. For larger α, a significant reduction in x_R is observed which is mainly caused by an upstream shift of the region in which instability waves grow exponentially. Mean flow profiles of U and V at the same normalized distance $(x - x_R)/H$ from reattachment collapse for different α, if normalized by $U_0 = C_0 \cos\alpha$. Both mean and fluctuating wall pressure scale on U_0^2 for $\alpha \leqslant 50°$. The introduction of sweep has little effect on the turbulence structure inside the free shear-layer. The most prominent differences among individual cases are found in the near-wall region. In accordance with Weber and Danberg [9] it was found that recovery into a two-dimensional boundary layer proceeds faster with increasing sweep angle.

The low Reynolds numbers concomitant to transition introduce additional effects which are absent in the high Reynolds number range for which asymptotic behaviour of turbulence properties can be expected [15]. Thus, in order to provide data which might be of use for testing and improvement of turbulence models it is highly desirable to investigate the flow over the swept step in the regime where it is fully turbulent. This is achieved by raising the Reynolds number to $Re_H = 5000$ and switching to different upstream conditions, namely a zero-pressure gradient TBL approaching the step instead of a laminar one as in the previous study.

The goals of the present study include (i) the exploration of the range of sweep angles for which the flow is approximately sweep independent, (ii) the investigation of scaling properties for flows with different sweep angles, and (iii) the identification of possible effects on the statistical turbulence structure resulting from the introduction of sweep.

2. Method and configuration

The physical parameters of the simulation series, which covers sweep angles $\alpha = 0°, 15°, 30°, 40°, 50°, 60°$, and $70°$, match the ones from the experimental study of Jovic and Driver [16,17]. The expansion ratio is $E \equiv h_{\text{out}}/h_{\text{in}} = 6H/5H = 1.2$.

For all sweep angles, the free stream Reynolds number $Re_H = C_0 H/\nu$ was kept at 5000. In order to explore possible Reynolds number influences two additional simulations were carried out for $\alpha = 40°$ and $\alpha = 60°$, this time keeping $Re_\alpha = Re_H \cos\alpha$ fixed at 5000.

Akselvoll and Moin [18] showed that the planar case ($\alpha = 0°$) can be accurately predicted using the LES method if the properties of the incoming TBL at the step edge match those of the experiment. Since the 'rescaling' method developed by Lund et al. [19] for the generation of turbulent inflow data can easily be generalized to handle sweep, it is appropriate to base the entire investigation on LES. The subgrid stresses are modeled with the dynamic Smagorinsky closure in the formulation of Lilly [20] without the need for a special treatment of the near-wall region since the viscous layer is resolved. Subgrid stresses play a minor role in the momentum budget and contribute primarily to the energy dissipation. For the meshes used in this study, the ratio of subgrid eddy viscosity and molecular viscosity hardly exceeds one.

The filtered, incompressible Navier–Stokes equations for the primitive variables $u,\ v,\ w,\ p$ are solved with a hybrid finite-difference/spectral method. Dealiasing is performed based on phase-shifting during substeps of the three-level Runge–Kutta time integration scheme. Terms involving derivatives along the y-coordinate are treated implicitly in time. A hybrid direct/iterative Poisson solver allows for efficient solution on massively parallel machines [21].

A rectangular computational domain of size $L_x \times L_y \times L_z = 20H \times 6H \times 6H$ is discretised in the x, y-plane in $N_x = 315$ and $N_y = 98$ non-equidistant meshes using second order central differences for a staggered variable arrangement. The non-dimensional spacing $\Delta x/H$ is 0.045 at the step edge, 0.066 at $x = 6H$ and 0.08 at the domain outlet. In the wall normal-direction the spacing $\Delta y/H$ is 0.008 along the bottom plate and 0.006 at $y = H$. Between $y = 0$ and $y = H$ a total of 47 meshes is distributed. In the additional simulation for $\alpha = 60°$ with $Re_H = 10000$ the resolution in x and y was increased to $N_x = 439$ and $N_y = 132$.

The flow is considered to be homogeneous along z which allows the use of periodic boundary conditions and approximation of the solution as a Fourier series with $N_z/2+1 = 33$ Fourier modes. For $\alpha = 0°$ and $\alpha = 40°$ the domain width and the number of modes were reduced to $L_z = 4H$ and $N_z/2 + 1 = 25$, respectively. The grid resolution upstream of the step normalized by $\nu/u_\tau = 0.0039H$ is $\Delta x^+ = 25,\ \Delta y^+ = 1.5$, and $\Delta z^+ = 21$.

The location of the inlet boundary of the computational domain results from a compromise among conflicting aspects. Due to the elliptic nature of the problem the flow in the potential region deviates from a uniform parallel flow for some distance upstream of the edge. This upstream influence depends on several aspects such as the expansion ratio and the size of the separation region. However, this effect does not seem to be very pronounced in the present configuration since the LES of [18] reproduced accurately the experiment of [17] despite the inlet plane being located as close as $0.3H$ to the edge.

In the case of sweep the situation is complicated by the fact that the evolution of the boundary layer with respect to x proceeds at a different rate for each angle α. In order to study the sweep influence on the separation region it is desirable to have comparable integral properties of the shear layer at the edge. This is most easily achieved by placing the inlet boundary as close as possible to the step. Given these conflicting aspects, we chose to locate the domain inlet boundary at $x = -1.5H$.

Unsteady inflow data was created for each sweep angle according to the similarity scaling method of Lund et al. [19] which has been modified to account for sweep as in Wu and Squires [4]. Before feeding the data stream from the inflow generator into the backstep simulation, the mean flow component $V(y)$ was adjusted such that it decreased from its peak value at the boundary layer edge near $y \approx 2.04H$ towards zero at $y = 6H$. The Reynolds number $Re_\theta = C_0\theta/\nu \approx 600$, the displacement thickness $\delta^* \approx 0.18H$, and the momentum thickness $\theta \approx 0.12H$ of the incoming turbulent boundary layer match the experiment of Jovic and Driver [16,17]. At the outflow boundary the advection equation

$$\frac{\partial u_i}{\partial t} + U_c \cos\alpha \frac{\partial u_i}{\partial x} + U_c \sin\alpha \frac{\partial u_i}{\partial z} = 0 \tag{9}$$

is solved with $U_c = 0.83C_0$ using third-order upwind differences as the approximation for the spatial derivatives.

The method was validated by comparison of first and second moments of the planar case with measurements [16] and DNS results [22]. For the planar case, the present LES predicts $x_R = 6.2H$ which deviates by less than 1.5% from the DNS.

3. Results

3.1. The swept turbulent boundary layer ahead of the step

The adaptation of the inflow generation method of Lund et al. [19] to the swept configuration poses no difficulties. But for two reasons, a zero pressure gradient swept TBL might develop differently from the un-swept case. As outlined in Section 1.2, physically, the situation might differ from a canonical TBL since the flow is no longer homogeneous with respect to the direction normal to the free stream. Another source for deviations from the un-swept case has to do with the numerical approximation: since the dispersive error of the numerical scheme depends on the relative orientation of the mean flow and the grid lines,

it is not to be expected that LES of a swept co-planar TBL yields identical results for every value of α. For DNS, the dispersive or phase error can be driven to zero by grid refinement since it affects primarily the high wave numbers. But for LES based on low-order central difference approximations this error is unavoidable unless one resorts to the expensive method of 'explicit filtering' [23]. Several studies have been devoted to the role of numerical errors in LES [24–27]. For the hybrid finite-difference/spectral scheme employed in this study, advection by the mean flow is actually predicted more accurately for high sweep angles compared to $\alpha = 0°$ since the Fourier approximation with respect to z is virtually free of phase errors.

Thus, prior to the study of flow separation we have to monitor the outcome of the inflow generation simulations. These simulations were carried out on Cartesian domains of size $L_x \times L_y \times L_z = 10H \times 5H \times 6H$ using $N_x \times N_y = 129 \times 53$ meshes and the same number of Fourier modes as the subsequent simulations of the flow over the step.

Figs. 2 and 3 show the results. The introduction of sweep has little effect on the outer parts of the profiles of mean velocity and turbulent shear stress. We observe a monotonic decrease in the magnitude of the near-wall peak of the stress profile as α

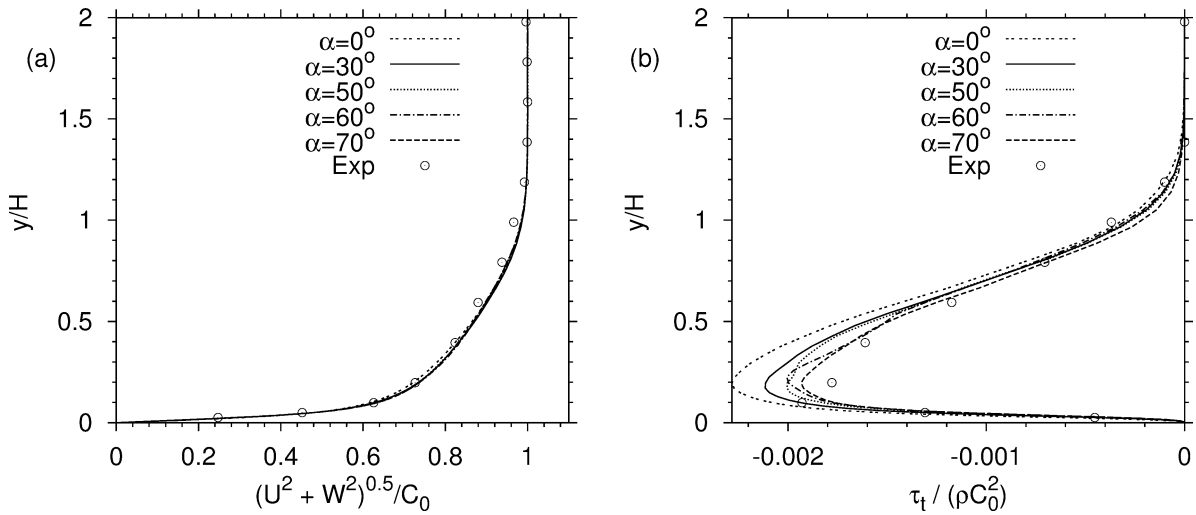

Fig. 2. Profiles of mean velocity $(U^2 + W^2)^{0.5}/C_0$ and turbulent shear stress $\tau_t/(\rho C_0^2) = -(\langle u'v'\rangle^2 + \langle v'w'\rangle^2)^{0.5}/C_0^2$ at $x/H = -1$ close to the domain inlet. Results at this station are very similar to the outcome of the inflow generation simulations. Circles denote measurements of [16].

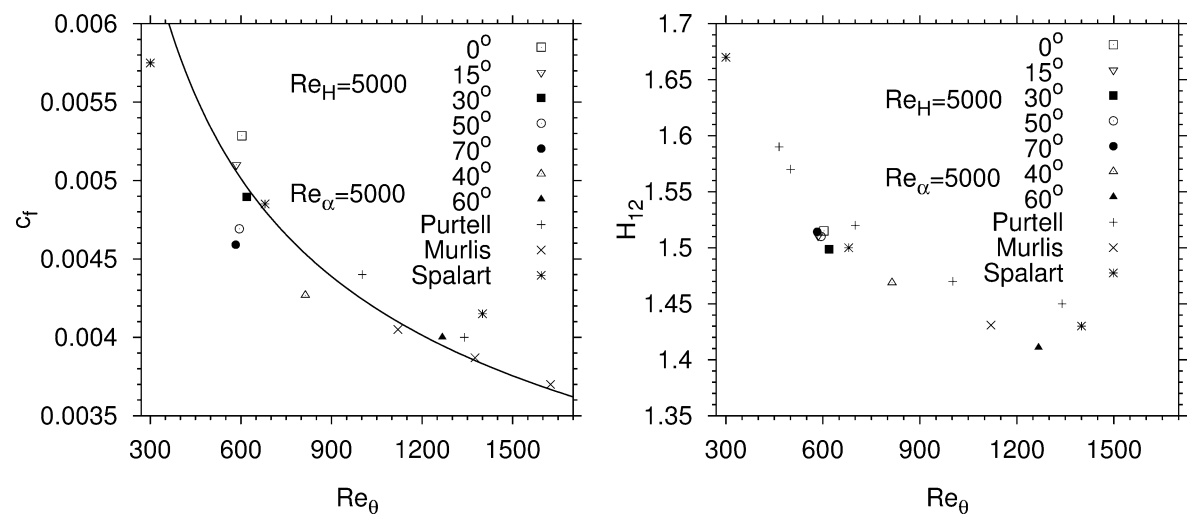

Fig. 3. Friction coefficient $c_f = \tau_W/(0.5\rho C_0^2)$ and shape factor $H_{12} = \delta^*/\theta$ as function of Reynolds number $Re_\theta = C_0\theta/\nu$ from turbulent inflow data at different α. Results are shown for $\alpha = 0°$, 15°, 30°, 50° and 70° for the series with $Re_H = 5000$ and for $\alpha = 40°$ and 60° for the series with $Re_\alpha = 5000$. Included are experimental data (various symbols), the empirical correlation described in [15] (—), and DNS results for the un-swept, zero pressure gradient TBL [37].

is increased. This is reflected in a slight decrease of the friction coefficient with increasing α which is shown in Fig. 3. The observed change in c_f is most likely a side-effect of the numerical approximation. This interpretation is backed by the outcome of an additional series of LES of turbulent channel flow: similar to the TBL, a slight decrease in c_f was observed when the mean pressure gradient was oriented in such a way that the resulting mean flow was no longer aligned with the grid.

Several studies show that the flow over the backward-facing is not very sensitive with respect to the properties of the upstream flow once it is fully turbulent. For example the DNS of [28] closely matched the experiment of [16] despite more than 30% differences in both Re_H and δ_{99}/H. Similarly, Adams et al. [29] found that in the range $8000 \leqslant Re_H \leqslant 26\,000$ the reattachment length x_R changed by $0.3H$ or less than 5% when δ_{99}/H varied between 0.6 and 1.6. Thus, since we managed to keep the integral parameters of the incoming TBL such as δ_{99}, δ^*, and θ within a relative narrow band we consider the turbulent inflow data used in this study to be of sufficient quality for the purpose of the investigation.

Fig. 3 includes data from the two additional simulations for $\alpha = 40°$ and $\alpha = 60°$ with $Re_\alpha = 5000$, respectively $Re_H = 6527$ and $Re_H = 10\,000$. The observed trends in c_f and H_{12} with increasing Re_θ are similar to the experimentally backed Reynolds number dependence of these parameters in the un-swept case. This gives further confidence in the suitability of the inflow generation method.

3.2. Mean flow and reattachment length

Fig. 4 shows the dependence of the reattachment length x_R on the sweep angle α. Up to $\alpha = 30°$, the reattachment length is little affected by the introduction of sweep which is in accordance with experiments [10,8,9]. For $\alpha > 30°$, x_R gradually decreases with a reduction by a third for $\alpha = 70°$ compared to the un-swept case. For $\alpha = 40°$, the two cases with either $Re_H = 5000$ or $Re_\alpha = 5000$ yield similar values of x_R, whereas for $\alpha = 60°$ the doubling of Re_H results in a 9% increase in x_R.

Compared to the transitional flow with laminar upstream conditions the decrease in x_R with increasing α is less pronounced for turbulent upstream conditions. Also, the decrease in x_R is much weaker than a cosine dependence. With $x_{R,\min} \approx 3.3H$ the minimum reattachment length is considerably smaller in the transitional case than in the swept turbulent case where $x_{R,\min} \approx 4H$, although we cannot exclude that a further reduction might result for $\alpha > 70°$.

For laminar upstream conditions the decrease in x_R is primarily caused by a shortening of the region in which transition takes place [5]. Additional aspects which might be partially responsible for the observed differences between the transitional and turbulent case are listed subsequently: (i) transitional flows tend to exhibit higher turbulence intensities than flows with fully developed turbulence [15], (ii) with $\theta/H \approx 0.03$ the shear layer thickness at the edge – which is one of the parameters governing the size of the reverse flow region [29] – is considerably smaller in the transitional case than in the turbulent case where $\theta/H \approx 0.12$, (iii) the expansion ratio in both configurations differs, and (iv) both series were carried out under different conditions for Re_α.

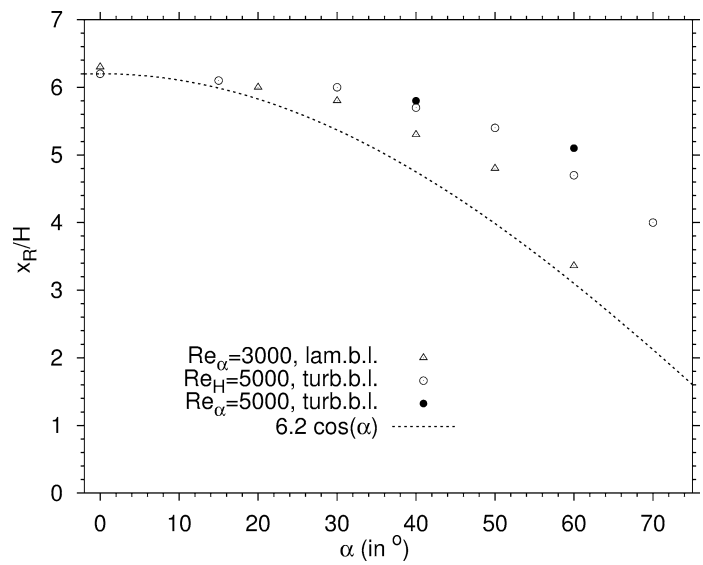

Fig. 4. Reattachment length x_R/H (normal to step) as function of sweep angle α. Included are results from LES for $Re_H = 5000$ and $Re_\alpha = 5000$ and DNS for $Re_\alpha = 3000$ from [5] (series B).

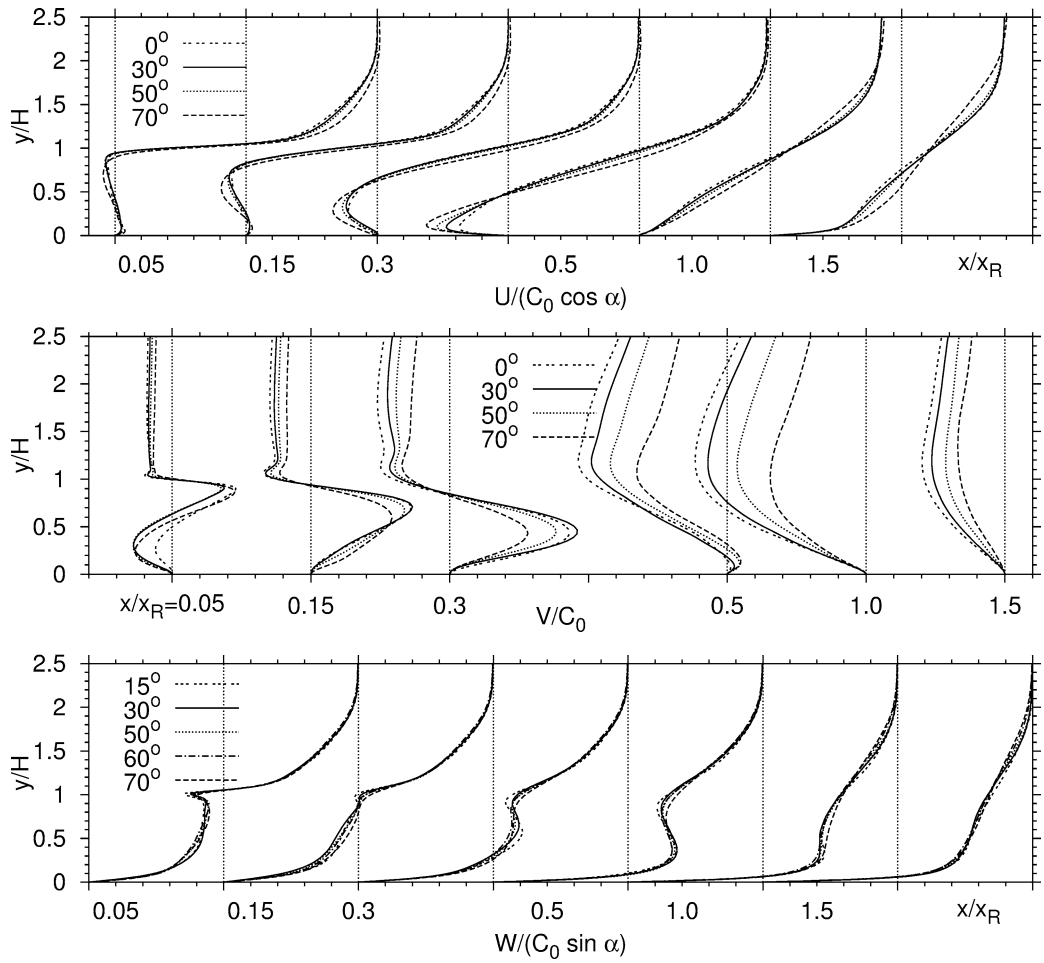

Fig. 5. From top to bottom: profiles at selected stations x/x_R as indicated below the horizontal axis for mean velocity components U/U_0, V/C_0 and W/W_0 with respect to coordinates x, y, z aligned with the step. The ticmark spacing along the horizontal axis is 0.1 for U and W and 0.01 for V.

Components of the mean flow decomposed with respect to the step-aligned coordinates x, z are shown in Fig. 5. The profiles are compared at the same non-dimensional location x/x_R since it is well established that the bubble length x_R is one of the relevant scales in separated flows [29–32]. At a given x/x_R, profiles of U normalized by $U_0 = C_0 \cos\alpha$ approximately collapse for sweep angles up to $\alpha = 50°$. The range of sweep angles, for which the normalized profiles $W/(C_0 \sin\alpha)$ approximately collapse extends up to $\alpha = 70°$. However, it would be wrong to infer from this type of approximate collapse that the sweep independence principle extends over the entire range of α considered. Strict sweep independence requires a collapse of profiles at the same distance x/H from the step which is no longer the case for $\alpha \geqslant 30°$ since x_R was found to decrease.

The V-profiles differ from the others with respect to the scaling: obviously, there is no single 'scale' which produces collapse in the entire region. Close to the step, V-profiles approximately fall on a single curve when normalized by C_0 whereas a better collapse (not shown) would result in the second half of the bubble if U_0 were used for normalization. Far downstream of reattachment V should scale again on C_0 which is consistent with the trend observed at the last two stations. The analysis of the scaling behaviour of V is complicated by the constraint $\partial V/\partial y = -\partial U/\partial x$ imposed by continuity in the x, y-plane together with the fact that x_R decreases for large sweep angles.

The observed scaling of V on C_0 violates the conditions for strict sweep independence. As outlined in Section 1.2, it does not preclude collapse of profiles U/U_0 and W/W_0 since it is consistent with a co-planar flow in which the Reynolds shear stresses satisfy certain scaling relations. However, the fact that the relevant scale for V shifts from C_0 towards U_0 indicates that changes in the scaling behaviour of the momentum balances (Eqs. (1)–(3)) take place. In other words: the collapse of profiles of U/U_0 and W/W_0 is not a sufficient criterion to arrive at the conclusion that the equilibrium of forces is approximately invariant with respect to the sweep angle.

The approximative collapse of mean velocity profiles has implications for the scaling of the wall shear stress components $\tau_{w,x}$ and $\tau_{w,z}$ which are shown in Fig. 6. The normalization of friction coefficients differs from the one used in the transitional case [5]. There, Re_α was kept constant whereas in the present series $Re_\alpha = Re_H \cos\alpha$ decreased with α. At the inlet of the domain, the step-normal and the step-parallel components of the wall shear stress follow from $\tau_{w,x} = \tau_w \cos\alpha$ and $\tau_{w,z} = \tau_w \sin\alpha$. Since the inflow generation yields $c_f = \tau_w/(0.5\rho C_0^2) \approx const.$, it follows that $c_{f,x} \equiv \tau_{w,x}/(0.5\rho C_0^2 \cos\alpha)$ and $c_{f,z} \equiv \tau_{w,z}/(0.5\rho C_0^2 \sin\alpha)$ are approximately constant at the domain inlet. Now, since the profiles U/U_0 approximately collapse for different sweep angles, the corresponding friction coefficients $c_{f,x}$ almost fall on a single curve as shown in Fig. 6. Similarly, the approximate collapse of W/W_0 profiles implies that curves of $\tau_{w,z}(x)$ exhibit a similar shape when normalized by $C_0^2 \sin\alpha$.

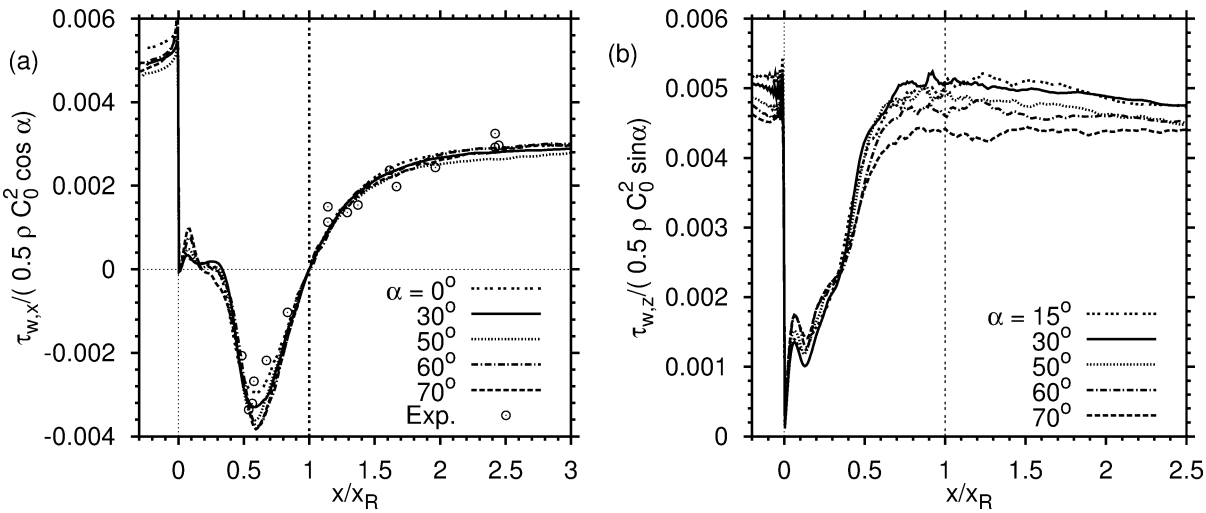

Fig. 6. Friction coefficients $\tau_{w,x}/(\rho C_0^2 \cos\alpha)$ and $\tau_{w,z}/(\rho C_0^2 \sin\alpha)$ as function of x/x_R.

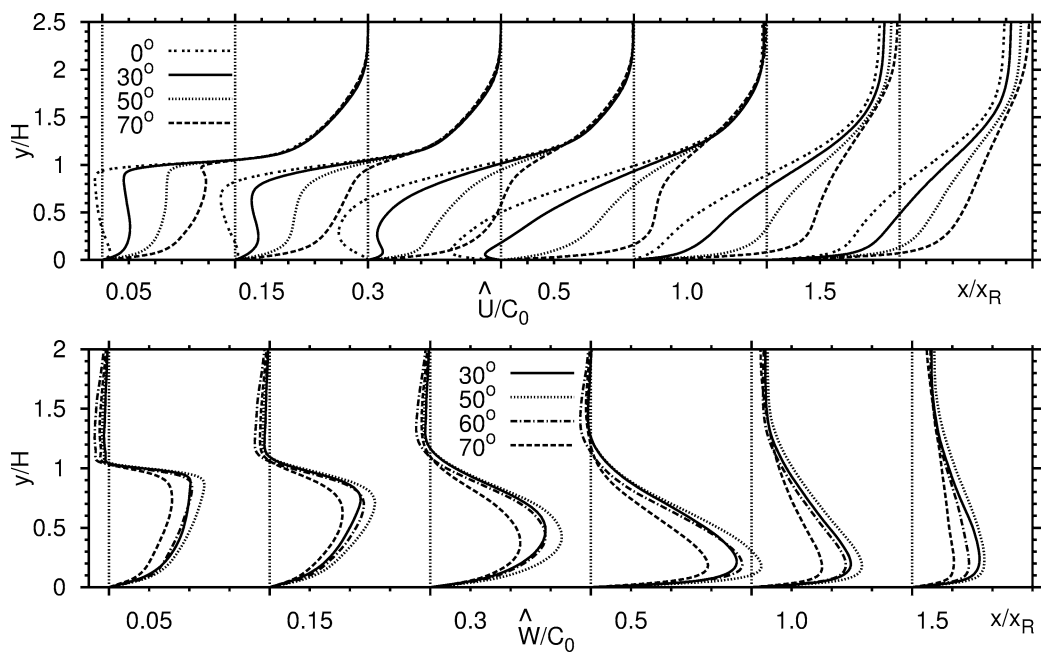

Fig. 7. Profiles at selected stations x/x_R as indicated below the horizontal axis for mean velocity components $\widehat{U}/C_0$ and $\widehat{W}/C_0$ with respect to coordinates $\hat{x}$ and $\hat{z}$ aligned with the free stream. The ticmark spacing along the horizontal axis is 0.1.

For all sweep angles, the (negative) peak in $c_{f,x}$ occurs near $x/x_R \approx 0.6$ independent of the fact that x_R is reduced for larger α. Similarly, all cases show that $c_{f,z}$ remains fairly constant throughout the reattachment region $0.7 < x/x_R < 1.5$. Thus, the change in the direction of wall streamlines occurring near x_R is primarily caused by the sign change of $c_{f,x}$ at x_R. Typical wall stream lines are shown in [13].

Both the flow decomposition into components $\widehat{U}$ and $\widehat{W}$ shown in Fig. 7 and the hodographs shown in Fig. 8 give an impression of the three-dimensional character of the mean flow. It becomes evident that reversed flow, i.e., a mean flow component opposite to the free stream, no longer occurs for $\alpha \geqslant 40°$. Two regions exist in which the mean flow is approximately aligned with the step edge: (i) for $y/H \leqslant 1$ the presence of the step face kinematically forces the mean flow near the step to turn, and (ii) near reattachment the vanishing of U causes the flow to become aligned with the attachment line which itself is parallel to the step.

A cross flow with a maximum magnitude $\widehat{W}/C_0 > 0.4$ is observed for angles $40° \leqslant \alpha \leqslant 60°$. It occurs near $x/x_R = 0.5$, i.e., close to the location where $c_{f,x}$ has its negative peak. The emergence of the maximum cross flow is related to the fact that in the region $0.6 \leqslant x/x_R \leqslant 0.9$ a substantial adverse pressure gradient $\partial P/\partial x$ exists which drives the near-wall low-momentum fluid towards the step. Since the pressure gradient acts in a direction which differs from that of the free stream, it induces

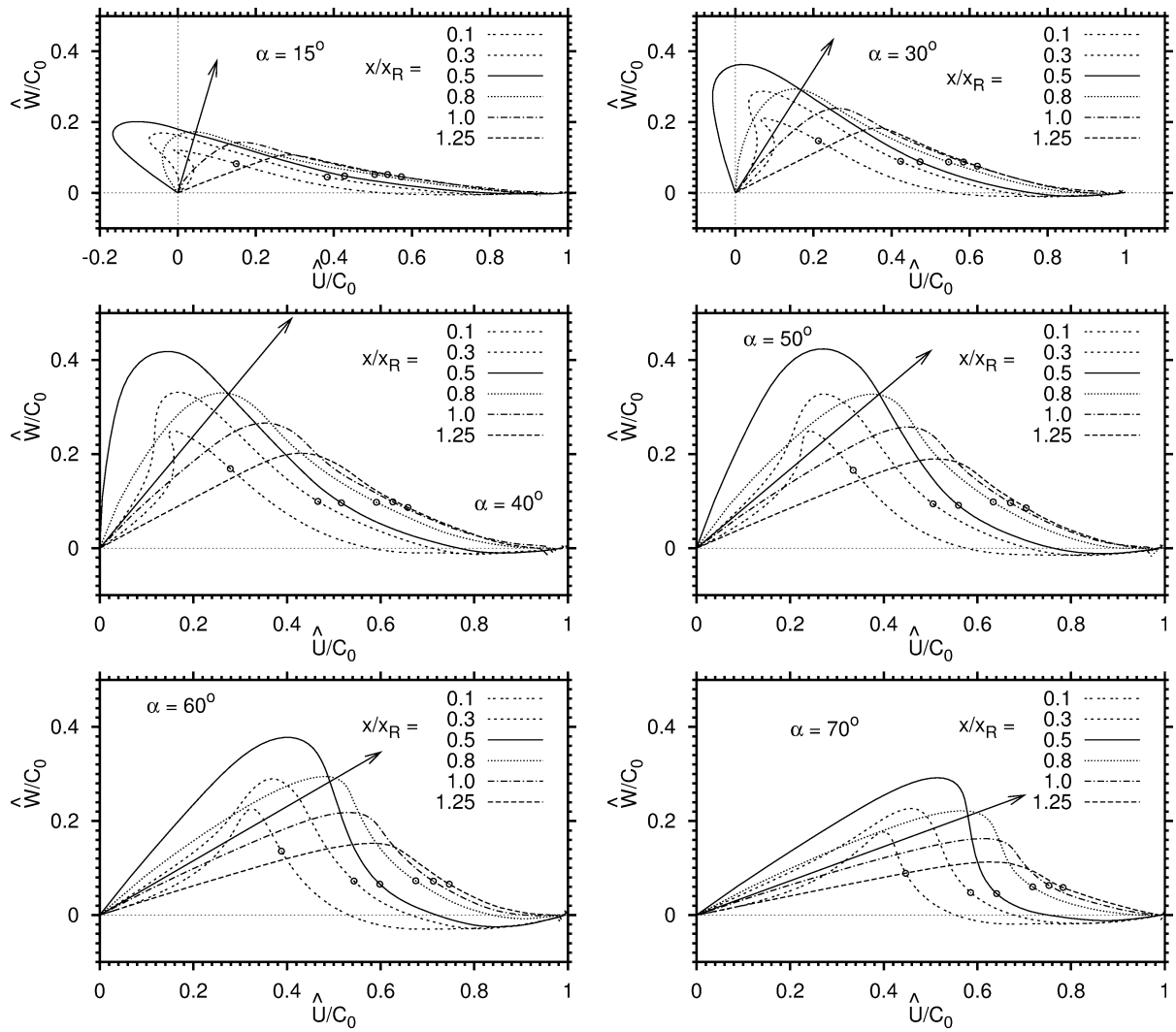

Fig. 8. Hodographs of the mean velocity vector at different streamwise positions x/x_R as marked in the legend. Circles denote a certain wall distance, namely $y/H = 0.95$ for $x/x_R \leqslant 0.3$ and $y/H = 0.9$ elsewhere. The arrows point in the direction of the z-axis. (For an observer looking from above on the configuration sketched in Fig. 1(right), i.e., in the direction of negative y, the axis for $\widehat{W}$ would have to point in the opposite direction.)

three-dimensionality in the mean flow. Fig. 9(b) shows that for $x/x_R > 0.6$ the magnitude of the maximum pressure gradient scales approximately on U_0^2. Thus the component $\partial P/\partial \hat{z}$ acting in the direction of the cross flow, scales on $C_0^2 \cos^2\alpha \sin\alpha$. This explains why both the skewing of the mean flow and the maximum of the cross flow tend to get weaker for $\alpha > 50°$ which becomes evident in the hodographs.

The profiles of $\widehat{W}$ give an impression how axial vorticity $\Omega_{\hat{x}} = \partial\widehat{W}/\partial y - \partial V/\partial\hat{z}$ is distributed in the flow. Initially, as a result of the sudden change in the wall boundary condition along the swept edge, $\Omega_{\hat{x}}$ is concentrated in the thin shear layer emanating from the step edge. Gradually, axial vorticity of opposite sign accumulates near the bottom wall and is reinforced through the 'sidewise' pressure gradient component $\partial P/\partial\hat{z}$. This flow cannot easily be classified according to the origin of axial vorticity since each of the three mechanisms which give rise to $\Omega_{\hat{x}}$ – spanwise shear, sidewise pressure gradient, and Reynolds stress gradients – play a role in this flow. Vorticity budgets are discussed in [13].

Both the mean wall pressure and the wall pressure fluctuations, which are shown in Figs. 9 and 10, provide further evidence that the scaling of this flow differs from the transitional case where both c_p and $c_{p'}$ based on U_0^2 approximately collapse [5]. Fig. 9(a) shows that the low pressure in the region $x/x_R < 0.5$ scales on $C_0^2\cos\alpha$ whereas Fig. 9(b) implies that the overall

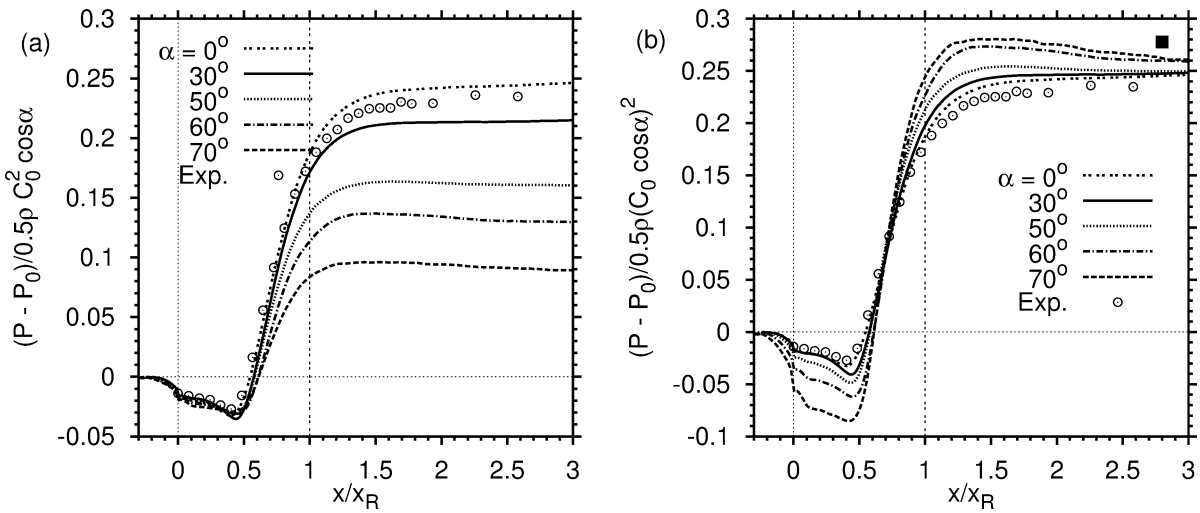

Fig. 9. Wall pressure coefficient c_p in two different normalizations versus x/x_R: $(P - P_0)/(0.5\rho C_0^2\cos\alpha)$ (a) and $(P - P_0)/(0.5\rho U_0^2)$ (b). The symbol (■) marks the prediction from the momentum integral theorem.

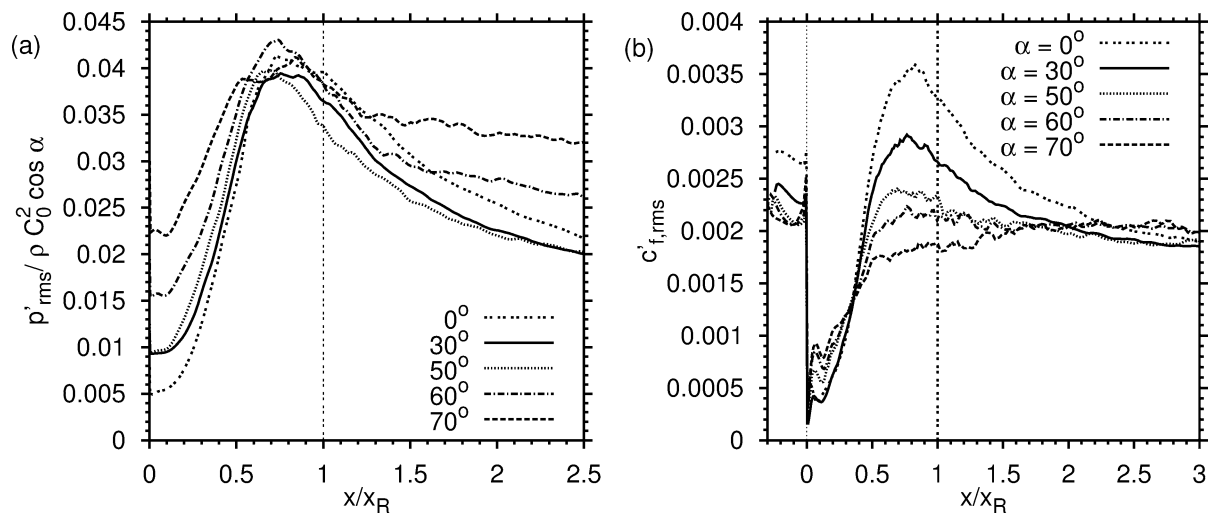

Fig. 10. (a) Root mean square $p'_{\rm rms}/(\rho C_0^2\cos\alpha)$ of wall pressure fluctuations; (b) rms of $c'_f = \tau'_w/(0.5\rho C_0^2)$ of the wall shear stress versus x/x_R. Note that different normalizations have been used in both plots.

increase in pressure scales approximately on U_0^2. The latter scaling is consistent with the momentum integral theorem which predicts that the pressure rise

$$c_{p,M} \equiv \frac{\Delta P}{0.5\rho U_0^2} = \frac{2}{E}\left(1 - \frac{1}{E}\right) \tag{10}$$

is a function of the expansion ratio E only. Fig. 9(b) shows that for $E = 1.2$ the predicted value $c_{p,M} = 0.28$ is slightly higher than the asymptotic value of the wall-pressure difference observed in the simulations.

In Section 1.2 it was shown that strict sweep independence requires each term in Eq. (1) to scale on $U_0^2 L_0^{-1}$. Thus, since $\partial P/\partial x$ is an important term in the momentum budget near reattachment, it is probably responsible for the fact that several flow quantities scale according to the criteria developed earlier, giving the (erroneous) impression that the sweep independence principle is applicable.

Friedrich and Arnal [33] observed that wall pressure fluctuations in the separation region behind a backward-facing step mirror the increase in turbulent kinetic energy (TKE) which takes place in the free shear layer. As a consequence of the inflow conditions, both the TKE $k = 0.5\langle u_i' u_i' \rangle$ and the rms $\langle p'^2 \rangle^{0.5}$ of wall pressure fluctuations scale on C_0^2 upstream of the step edge and in a short region downstream of it. The same scaling applies again far downstream of the reattachment location. Fig. 10(a) shows that in the intermediate region a change in scaling takes place since the maximum rms value that occurs slightly upstream of reattachment, scales on $C_0^2 \cos\alpha$. Turbulent fluctuations undergo similar changes in scaling. This can be inferred from Fig. 10(b) which shows that the rms of the fluctuating wall shear stress scales on C_0^2 both upstream of the step and far downstream of reattachment, whereas a better collapse (not shown) would result in the region $0.5 < x/x_R < 1.5$ if $C_0^2 \cos\alpha$ were used for normalization.

From the modeling point of view it is important to know how skewing of the mean flow might affect the evolution of turbulence. Since the turbulence production occurs primarily in regions with high shear rates, it is useful to study these regions in more detail. Fig. 11(a) shows that upstream of $x/x_R = 0.3$, the maximum of the 'vertical' shear rate $S = [(\partial U/\partial y)^2 + (\partial W/\partial y)^2]^{0.5}$ occurs slightly above $y = H$. Both, the hodographs shown in Fig. 8 and the profiles shown in Fig. 7 imply that the skewing of the mean flow profiles is not very pronounced in this particular region. Thus, possible side-effects from the three-dimensionality of the mean flow might be small inside the free shear-layer region.

A useful measure for this type of effect is the lag angle $\gamma_{\text{lag}} = \gamma_{u'v'} - \gamma_S$ which quantifies the misalignment of shear-stress and velocity-gradient vectors. Here, the definitions

$$\gamma_{u'v'} = \arctan\left(\frac{\langle v'w' \rangle}{\langle u'v' \rangle}\right), \qquad \gamma_S = \arctan\left(\frac{\partial W/\partial y}{\partial U/\partial y}\right) \tag{11}$$

have been used. Fig. 11(c) shows that γ_{lag} hardly exceeds 20° in the region where the shear rate S is highest. Larger values of γ_{lag} do occur in the flow but they seem to be confined to regions in which the shear rate and therefore the production terms for the Reynolds stresses are small. This is consistent with the observation of Wu and Squires [4] who found that models which rely on the alignment of shear-stress vector and velocity-gradient vector assuming an isotropic eddy viscosity do not necessarily fail in three-dimensional flows.

Another aspect which makes the swept cases different from the planar backstep, is the emergence of the non-diagonal, rotational strain rate component $S_{13} = 0.5\partial W/\partial x$ which acts in the wall-parallel plane. However, Fig. 11(b) shows that in regions with large 'vertical' shear rate S the magnitude of the 'horizontal' shear rate remains relatively small. Thus, similar to [2] we arrive at the conclusion that it is often difficult to identify a specific influence of the three-dimensional character of the strain rate tensor on the turbulence evolution.

3.3. Turbulence structure

In this section structural changes of turbulence are identified in a statistical sense by a description of the evolution of the Reynolds stress tensor. In the following, all evaluations are based on the resolved velocity field. Since in these simulations the subgrid stresses contribute little to the total stresses, they can be safely neglected without biasing the conclusions.

Fig. 12 gives an impression of the evolution of the Reynolds stresses. In general, none of the depicted quantities which include the TKE and the kinematic shear stresses $\langle u'v' \rangle$ and $\langle v'w' \rangle$ exhibit a good collapse for *all* sweep angles at *all* locations considered. Other scalings such as U_0^2 for $\langle u'v' \rangle$ and $U_0 W_0$ for $\langle v'w' \rangle$, used in [34], do improve the collapse (not shown) in the vicinity of reattachment. This suggests that it might not be possible to capture the influence of sweep entirely in terms of simple scaling laws. Nevertheless, a few useful conclusions can be drawn.

The flow dynamics are governed by the strong growth of turbulent fluctuations in the initial region ($x < 1.5H$) of the free shear layer emanating from the edge. The term $\partial\langle u'u' \rangle/\partial x$ contributes little to Eq. (1). Therefore and because of $\langle u'v' \rangle_{\max} = -\int_{y_{\max}}^{\infty} (\partial\langle u'v' \rangle/\partial y)\,\mathrm{d}y$ the peak value of the shear stress $-\langle u'v' \rangle$ occurring at $y_{\max} \approx H$ can be interpreted as

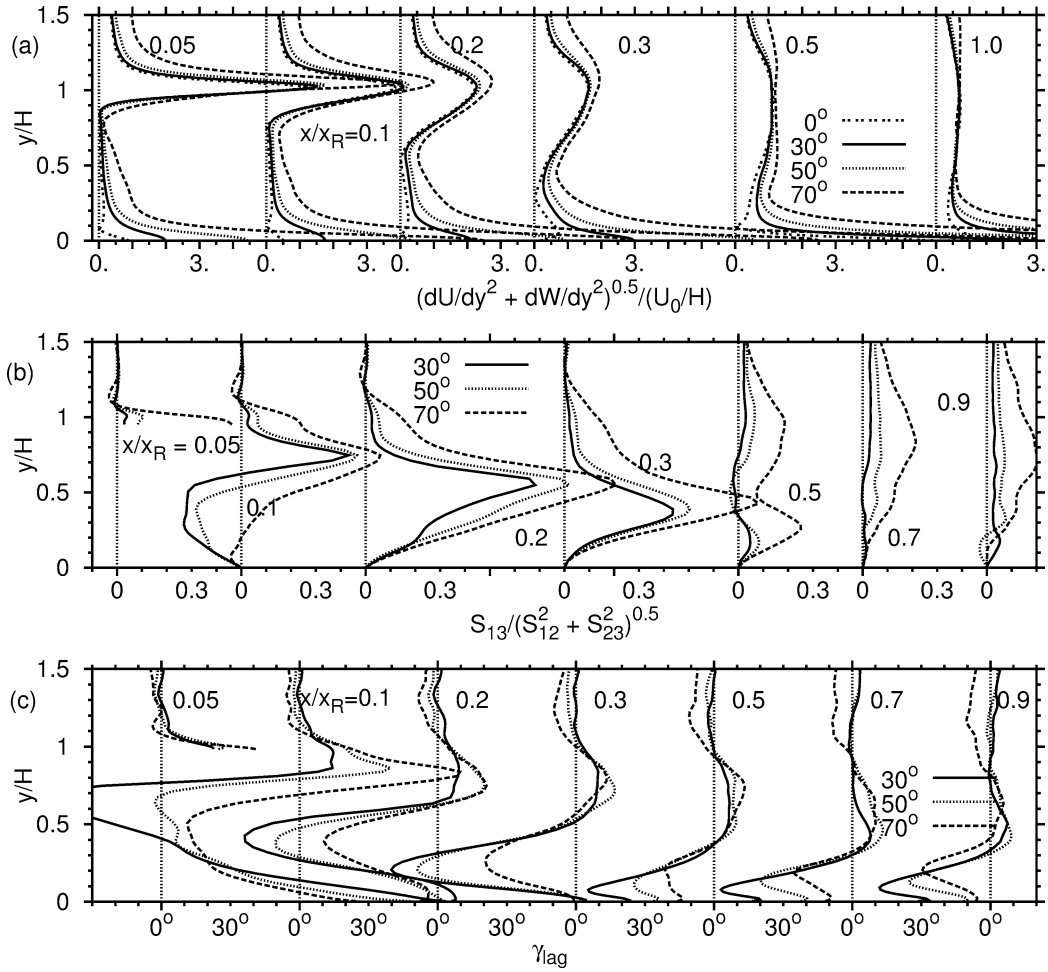

Fig. 11. (a) Magnitude $[(\partial U/\partial y)^2 + (\partial W/\partial y)^2]^{0.5}/(C_0 \cos\alpha/H)$ of the velocity gradient vector, (b) ratio $S_{13}/(S_{12}^2 + S_{23}^2)^{0.5}$ of strain-rate tensor components, (c) lag angle $\gamma_{\text{lag}} = \gamma_{u'v'} - \gamma_S$ between shear-stress vector and velocity-gradient vector at selected stations x/x_R.

the total of the decelerating force exerted by the turbulence with respect to the x-direction. Fig. 13(a) shows that all cases experience a similar fivefold increase in the magnitude of this force. Figs. 12(b) and 13(a) show that $C_0^2 \cos\alpha$ remains the relevant 'scale' for the normalization of this stress tensor component up to $x \approx 2H$. Near reattachment, $\langle u'v' \rangle$ shows a trend to scale on U_0^2 similar to the transitional case [5]. As discussed earlier, this might be related to the fact that the adverse pressure gradient $\partial P/\partial x$ scales on U_0^2 due to the constraints imposed by the momentum integral theorem.

The analysis of the scaling behaviour of the Reynolds stresses is complicated by the fact that the distance over which a certain scaling applies appears to be different for each quantity considered. For example, Fig. 13(b) shows that the peak value of the wall normal variance $\langle v'v' \rangle$ scales on C_0^2 only in the short region $x < 0.5H$. Further downstream, $C_0^2 \cos\alpha$ is more appropriate (not shown) for the scaling of $\langle v'v' \rangle$.

Profiles of the TKE show a similar change in scaling as the variance $\langle v'v' \rangle$. Except for the cases with high sweep angles ($\alpha \geqslant 60°$) the TKE profiles are dominated by a single peak which forms in the region of maximum vertical shear S. Fig. 12(a) shows that up to $\alpha = 50°$, this peak scales roughly on $C_0^2 \cos\alpha$ with the exception of the first station. There, due to the choice of the upstream conditions the peak of the TKE has to scale on C_0^2.

Probably the most persistent scaling is observed for the shear stress component $\langle v'w' \rangle$ which is shown in Fig. 12(c). Whereas profiles of $\langle v'w' \rangle$ normalized by $C_0^2 \sin\alpha$ show approximate collapse up to $x/x_R = 0.5$, the scaling of $\langle u'v' \rangle$ differs already at the mid-bubble position from the one further upstream. Again, we can refer to the special situation for the x-component of the momentum budget brought in by the adverse pressure gradient to explain these differences. Similar to $\langle u'v' \rangle$, near reattachment there is a tendency for the $\langle v'w' \rangle$ profiles to scale as in the transitional case, namely on $C_0^2 \cos\alpha \sin\alpha$ instead of $C_0^2 \sin\alpha$.

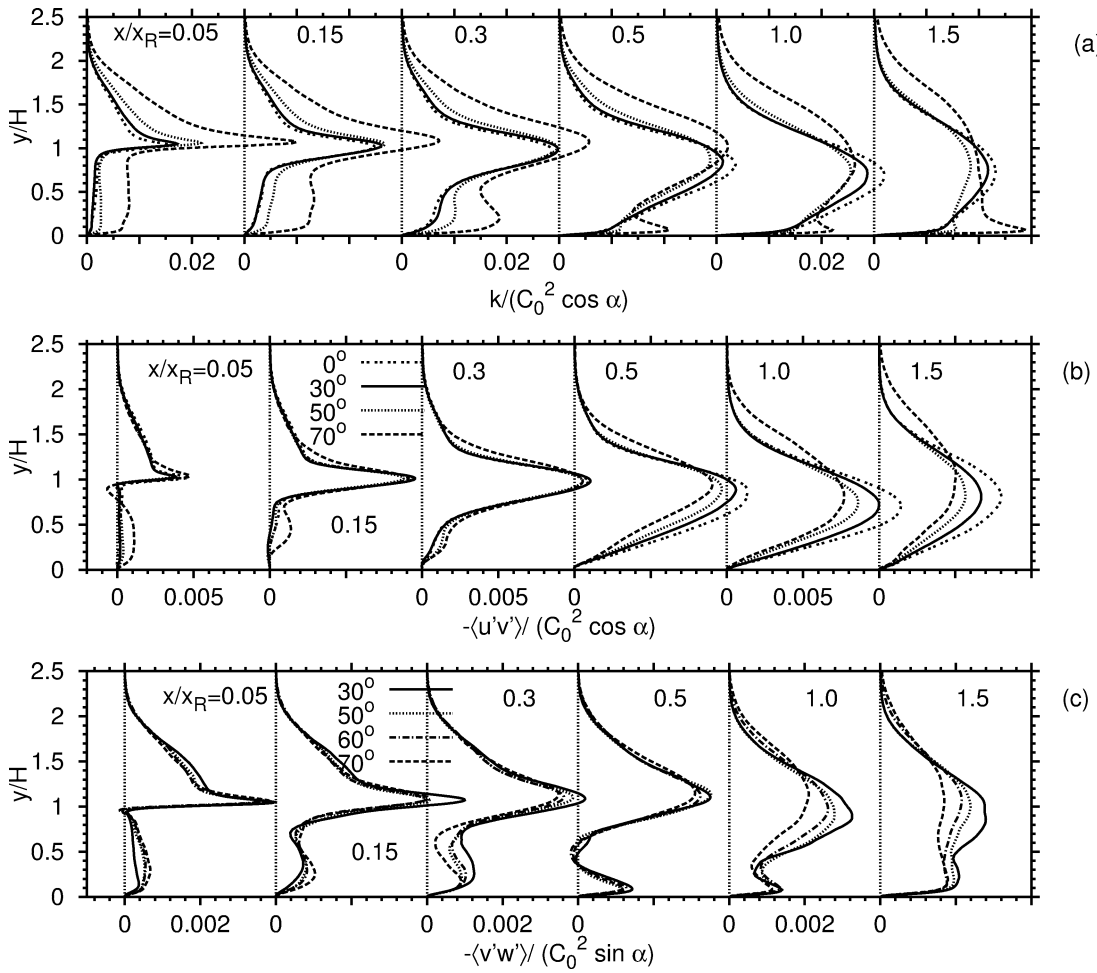

Fig. 12. (a) Turbulent kinetic energy $0.5\langle u_i' u_i' \rangle/(C_0^2 \cos\alpha)$, (b) Reynolds shear stresses $-\langle u'v' \rangle/(C_0^2 \cos\alpha)$, and (c) $-\langle v'w' \rangle/(C_0^2 \sin\alpha)$.

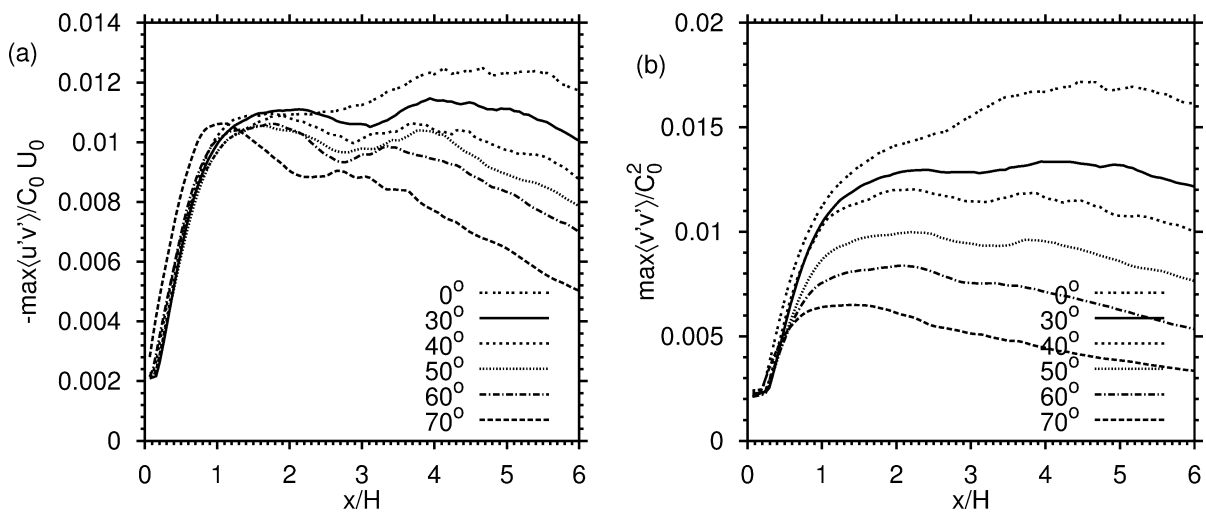

Fig. 13. Peak values of profiles $-\langle u'v' \rangle/(C_0^2 \cos\alpha)$ (a) and $\langle v'v' \rangle/C_0^2$ (b) from the free shear layer behind the edge versus x/H.

The two cases with $\alpha \geqslant 60°$ differ in one aspect from the others, namely the occurrence of a near-wall peak in profiles of the TKE well upstream of reattachment. This is particularly evident in the case $\alpha = 70°$ for which secondary peaks are clearly visible already at $x/x_R = 0.3$. Similar observations were made in [13] for the transitional case and the following explanation was offered: with increasing sweep angle α, the step-parallel component of the mean flow provides sufficient shear $\partial W/\partial y$ near the wall to sustain turbulence production. Apparently, this process is not much affected by the outer flow being highly disrupted by the turbulence evolution inside of the free shear layer. Further evidence for this interpretation came from the observation of streaks *upstream* of the reattachment location in case of high sweep angles [13].

Given the relatively complex three-dimensional flow and strain-rate fields it is interesting to monitor possible changes of the statistical turbulence structure. For this purpose, the structure parameters

$$a_1 = \frac{(\langle u'v'\rangle^2 + \langle v'w'\rangle^2)^{0.5}}{2k}, \qquad a_3 = \frac{\langle v'v'\rangle}{(\langle u'v'\rangle^2 + \langle v'w'\rangle^2)^{0.5}} \tag{12}$$

are shown in Fig. 14. If we focus our attention on the region $y > 0.9$ H with significant vertical shear S, it becomes evident that the parameter a_1 is not much affected by the introduction of sweep. Inside the free shear layer a_1 reaches peak values close to 0.19. The relaxation towards an equilibrium value – in the outer part of a canonical TBL $a_1 \approx 0.15$ – proceeds slowly. Similar to the transitional case [13], near the wall a slight tendency towards higher values of a_1 with increasing sweep angle can be observed at some stations.

Differences among individual cases are more pronounced with respect to the parameter a_3. However, the seemingly large influence of α on a_3 at stations $0.1 \leqslant x/x_R \leqslant 0.2$ is probably not very relevant since it occurs outside the region with large vertical shear. A persistent sweep influence on the magnitude of a_3 is observed near the wall. Here, the monotonic decrease in the magnitude and the off-wall shift of the peak value of a_3 signals a fundamental change in the turbulence structure which is caused by the increasing dynamical role of the strain rate S_{23}.

An alternate way for the identification of structural changes consists in the analysis of invariant maps of the Reynolds stress anisotropy tensor $b_{ij} = \langle u_i' u_j'\rangle/(2k) - \delta_{ij}/3$ as proposed in [35]. In Fig. 15, hodographs of the second and the third invariants $\mathrm{II} = -0.5 b_{ij} b_{ij}$ and $\mathrm{III} = (b_{ij} b_{jk} b_{ki})/3$ of the anisotropy tensor are plotted with the distance from the wall varying along each curve.

A characteristic feature of wall-bounded turbulence is the formation of an extremal state in the anisotropy map which is related to the emergence of alternating streaks of low speed and high speed fluid. This state occurs close to the straight two-component (2C) line from which all curves start for $y = 0$. In turbulent channel flow at $Re_\tau = 180$ the maximum deviation from the isotropic state $\mathrm{II} = \mathrm{III} = 0$ is found at a wall distance $y^+ = 3.5$ and corresponds to $-\mathrm{II} = 0.245$ and $\mathrm{III} = 0.044$ [36].

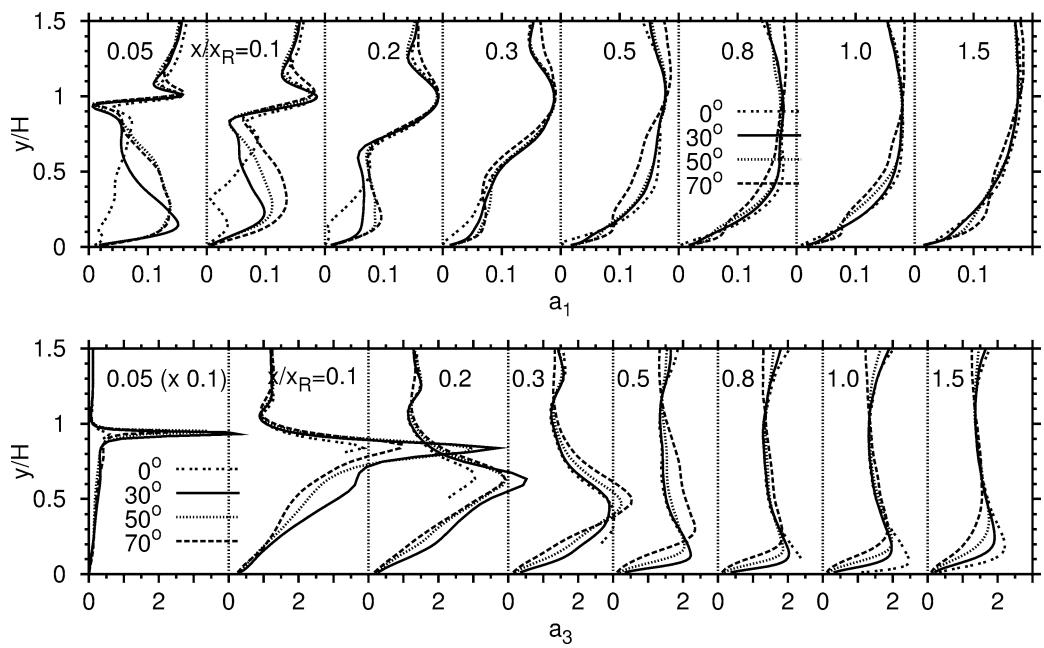

Fig. 14. Structure parameters a_1 and a_3 at selected stations x/x_R. Curves of a_3 at the station $x/x_R = 0.05$ have been multiplied by 0.1. For $\alpha = 0°$ the lower part of a_3-profiles has been clipped since this quantity becomes ill-conditioned in regions with vanishing shear stress.

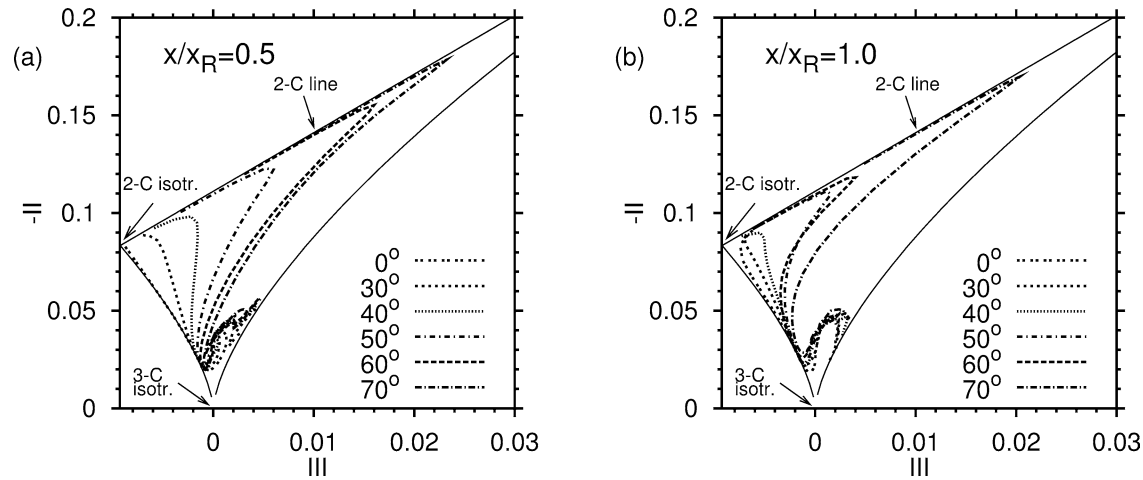

Fig. 15. Anisotropy invariant map of the Reynolds stress tensor at stations $x/x_R = 0.5$ (a) and $x/x_R = 1.0$ (b).

The most prominent difference between individual cases in Fig. 15 is concerned with this near-wall extremal state. Close to the 2C-line, hodographs tend to form a bulge which is oriented towards the 1C-corner of the diagram. This bulge gets more pronounced as the sweep angle increases. In the reversed flow region, the planar case ($\alpha = 0°$) behaves differently from the swept flows since its anisotropy state remains close to the axisymmetric state represented by the lower left boundary of the 'triangle'.

As previously noticed for the structure parameters a_1 and a_3, outside the near-wall region there seem to be hardly any differences in the turbulence structure between the planar and swept cases. This observation might be interpreted in the sense that the processes associated with the formation, growth, and reattachment of the free shear layer impose an 'overwhelming' influence on the turbulence evolution, thereby possibly masking weaker effects which result from skewing of the mean flow.

4. Conclusion

The flow over a swept, backward-facing step at $Re_H = 5000$ has been studied using large-eddy simulation for sweep angles up to $\alpha = 70°$. The reattachment length x_R remains nearly constant up to $\alpha = 30°$ and gradually decreases for higher angles. The introduction of sweep causes the mean flow to become strongly skewed inside the separation region. A maximum cross flow of 40% of the free stream velocity C_0 is observed shortly upstream of the region where the mean adverse pressure gradient reaches its maximum.

The decomposition of the flow into step-normal and edge-parallel components U and W, respectively, together with normalization by $U_0 = C_0 \cos\alpha$ and $W_0 = C_0 \sin\alpha$ shows approximate collapse if profiles are compared at the same normalized distance x/x_R. In previous studies, the invariance of x_R together with the observed scaling of mean flow profiles was interpreted in the sense that the sweep-independence principle holds over a certain range of sweep angles for the flow over a swept step and similar spanwise invariant flows.

Our results indicate that this interpretation is somewhat misleading. Firstly, in a strict sense the sweep-independence principle holds only in a laminar flow. Secondly, closer examination of the scaling properties of individual terms in the mean momentum balance reveals that the flow is far from being sweep independent. In fact, most quantities except for the profiles of U and W indicate that a change in scaling takes place.

The scaling imposed by the turbulent upstream conditions remains valid over a certain distance downstream of the edge. However, the distance over which this initial scaling holds differs for each quantity considered. For example, shear stresses scale as $\langle u'v'\rangle/(C_0^2\cos\alpha)$ and $\langle v'w'\rangle/(C_0^2\sin\alpha)$ in the first half of the separation bubble. Conversely, profiles of $\langle v'v'\rangle$ deviate from the initial scaling on C_0^2 as early as $x/x_R \approx 0.2$. Part of the observed change in scaling can be contributed to the adverse pressure gradient $\partial P/\partial x$ which becomes large in the second half of the bubble and which scales on U_0^2 in accordance with the momentum integral theorem.

No significant changes in the statistical turbulence structure are found due to the introduction of sweep except for the near-wall region. A possible explanation comes from the observation that the additional strain rates resulting from the introduction of sweep are relatively weak when compared with the vertical shear in the free shear layer. Near the wall, the situation is different

since inside the reverse flow region near-wall shear rates are moderate in the planar case. There, the existence of an additional shear rate provided by the spanwise flow can have a major effect on turbulence evolution.

It will be interesting to analyse how statistical turbulence models cope with the prediction of the subtle changes which result from the introduction of sweep. Possibly, this data set can help to establish criteria under which full second-order closures should be used instead of two-equation models.

Acknowledgements

Dipl. Phys. Werner Jürgens contributed valuable comments on a draft of the manuscript. Part of this work was funded by the Deutsche Forschungsgemeinschaft through the collaborative research center SFB 557. Computer time was provided by the Konrad-Zuse-Zentrum (ZIB) Berlin.

References

[1] J.P. Johnston, K.A. Flack, Review – advances in three-dimensional turbulent boundary layers with emphasis on the wall-layer region, J. Fluids Engrg. 118 (1996) 219–232.
[2] G.N. Coleman, J. Kim, P.R. Spalart, A numerical study of strained three-dimensional wall-bounded turbulence, J. Fluid Mech. 416 (2000) 75–116.
[3] D. Webster, D. Degraaff, J.K. Eaton, Turbulence characteristics of a boundary layer over a swept bump, J. Fluid Mech. 323 (1996) 1–22.
[4] X. Wu, K.D. Squires, Prediction of the three-dimensional turbulent boundary layer over a swept bump, AIAA J. 36 (1998) 505–514.
[5] H.-J. Kaltenbach, G. Janke, Direct numerical simulation of flow separation behind a swept, rearward-facing step at $Re_H = 3000$, Phys. Fluids 12 (2000) 2320–2337.
[6] P. Bradshaw, Turbulent secondary flow, Annu. Rev. Fluid Mech. 19 (1987) 53–74.
[7] H.-H. Fernholz, G. Janke, M. Kalter, M. Schober, On the separated flow behind a swept backward-facing step, in: K. Gersten (Ed.), Physics of Separated Flows – Numerical, Experimental and Theoretical Aspects, in: NNFM, vol. 40, Vieweg, Braunschweig, 1993, pp. 200–207.
[8] G.V. Selby, Applicability of the independence principle to subsonic turbulent flow over a swept rearward-facing step, AIAA J. 21 (11) (1983) 1603–1604.
[9] D.J. Weber, J.E. Danberg, Correlation of mean velocity measurements downstream of a swept backward-facing step, AIAA J. 30 (1992) 2701–2706.
[10] F.D. Barkey Wolf, Swept and unswept separation bubbles, Ph.D. thesis, University of Cambridge, 1987.
[11] P.E. Hancock, Measurements of mean and fluctuating wall shear stress beneath spanwise-invariant separation bubbles, Exp. Fluids 27 (1999) 53–59.
[12] J.R. Hardman, P.E. Hancock, The near-wall layer beneath a moderately converging three-dimensional turbulent separated and reattaching flow, Eur. J. Mech. B. Fluids 19 (2000) 653–672.
[13] H.-J. Kaltenbach, The effect of sweep-angle variation on the turbulence structure in a separated, three-dimensional flow, Theor. Comput. Fluid Dynamics 16 (3) (2003) 187–210.
[14] W. Jürgens, H.-J. Kaltenbach, Eigenmode decomposition of turbulent velocity fields behind a swept, backward-facing step, J. Turbulence 4 (2003) 018.
[15] H.-H. Fernholz, P.J. Finley, The incompressible zero-pressure gradient turbulent boundary layer: an assessment of the data, Prog. Aerosp. Sci. 23 (1996) 245–311.
[16] S. Jovic, D. Driver, Backward-facing step measurements at low Reynolds number, $Re_h = 5000$, Tech. Rep. NASA TechMemo 108807, NASA, 1994.
[17] S. Jovic, D. Driver, Reynolds number effects on the skin frirction in separated flows behind a backward facing step, Exp. Fluids 18 (1995) 464.
[18] K. Akselvoll, P. Moin, Large eddy simulation of turbulent confined coannular jets and turbulent flow over a backward facing step, Tech. Rep. TF-63, Thermosciences Division, Dept. of Mech. Engineering, Stanford University, Stanford, CA 94305, 1995.
[19] T.S. Lund, X. Wu, K.D. Squires, Generation of turbulent inflow data for spatially-developing boundary layer simulations, J. Comput. Phys. 140 (1998) 233–258.
[20] D.K. Lilly, A proposed modification of the Germano subgrid-scale closure method., Phys. Fluids A 4 (3) (1992) 633–635.
[21] H.-J. Kaltenbach, A. Jäkel, A hybrid direct/iterative algorithm for solution of Poisson's equation based on the Schur complement method, in: M. Breuer, F. Durst, C. Zenger (Eds.), High Performance Scientific and Engineering Computing, Proceedings of the 3rd International FORTWIHR Conference on HPSEC, Erlangen, March 12–14, 2001, Universität Erlangen, Springer, 2002, pp. 175–182.
[22] H. Le, P. Moin, J. Kim, Direct numerical simulation of turbulent flow over a backward-facing step, J. Fluid Mech. 330 (1997) 349–374.
[23] T. Lund, H.-J. Kaltenbach, Experiments with explicit filtering for LES using a finite-difference method, in: CTR Annual Research Briefs 1995, Center for Turbulence Research, Stanford Univ./NASA Ames Research Center, 1995, pp. 91–105.
[24] S. Ghosal, An analysis of numerical errors in large-eddy simulation of turbulence, J. Comp. Phys. 125 (1996) 187–206.
[25] A. Kravchenko, P. Moin, On the effect of numerical errors in large-eddy simulation of turbulent flows, J. Comp. Phys. 130 (1997) 310–322.

[26] H.-J. Kaltenbach, D. Driller, LES of wall-bounded turbulence based on a 6th-order compact scheme, in: B. Geurts, R. Friedrich, O. Métais (Eds.), Direct and Large-Eddy Simulation IV, Kluwer Academic, Dordrecht, The Netherlands, 2001, pp. 37–44.
[27] H.-J. Kaltenbach, D. Driller, Phase-error reduction in large-eddy simulation using a compact scheme, in: R. Friedrich, W. Rodi (Eds.), Advances in LES of Complex Flows, Proceedings of the Euromech Colloquium 412, held in Munich, Germany, 4–6 October 2000, Kluwer Academic, Dordrecht, The Netherlands, 2000, pp. 83–98.
[28] J. Neumann, H. Wengle, Passive versus active control of backward-facing step flow: DNS/LES and POD analysis, in: I. Castro, P. Hancock, T. Thomas (Eds.), Advances in Turbulence IX, Proceedings of the Ninth European Turbulence Conference, held in Southampton, July 2–5, 2002, Internat. Center for Numer. Methods in Engrg. (CIMNE), Gran Capitan s/n, 08034 Barcelona, Spain, 2002, pp. 573–576.
[29] E.W. Adams, J.P. Johnston, J.K. Eaton, Experiments on the structure of turbulent reattaching flow, Tech. Rep. MD-43, Thermosciences Division, Dept. of Mech. Engineering, Stanford University, Stanford, CA 94305, 1984.
[30] P. Bradshaw, F.Y.F. Wong, The reattachment and relaxation of a turbulent shear layer, J. Fluid Mech. 52 (1972) 113–135.
[31] I.P. Castro, A. Haque, The structure of a turbulent shear layer bounding a separation region, J. Fluid Mech. 179 (1987) 439–468.
[32] P.E. Hancock, Low Reynolds number two-dimensional separated and reattaching turbulent shear flow, J. Fluid Mech. 410 (2000) 101–122.
[33] R. Friedrich, M. Arnal, Analysing turbulent backward-facing step flow with the lowpass-filtered Navier–Stokes equations, J. Wind Engrg. Industr. Aerodynam. 35 (1990) 101–128.
[34] H.-J. Kaltenbach, The swept backward-facing step with an upstream turbulent boundary layer, in: I.P. Castro, P.E. Hancock, T.G. Thomas (Eds.), Advances in Turbulence IX: Proceedings of the Ninth European Turbulence Conference, held in Southampton, July 2–5, 2002, Internat. Center for Numer. Methods in Engrg. (CIMNE), Gran Capitan s/n, 08034 Barcelona, Spain, 2002, pp. 73–76.
[35] J.L. Lumley, G.R. Newman, The return to isotropy of homogeneous turbulence, J. Fluid Mech. 82 (1977) 161–178.
[36] N.N. Mansour, J. Kim, P. Moin, Reynolds-stress and dissipation rate budgets in a turbulent channel flow, J. Fluid Mech. 194 (1988) 15–44.
[37] P.R. Spalart, Direct simulation of a turbulent boundary layer up to $Re_\theta = 1410$, J. Fluid Mech. 187 (1988) 61.